DESIGN GUIDELINES FOR GUIDED-WAVE STRUCTURAL HEALTH MONITORING SYSTEMS USING PIEZOELECTRIC TRANSDUCERS

Ajay Raghavan, ajayr@umich.edu
Carlos E.S. Cesnik, cesnik@umich.edu
Department of Aerospace Engineering, The University of Michigan, 1320 Beal Avenue, Ann Arbor, Michigan 48105, U.S.A.

Abstract. *Several laboratory studies have examined structural health monitoring (SHM) using guided waves (GWs) excited by an onboard transducer network. However, possibly due to the incipient nature of this technology, often the various parameters involved are chosen without mathematical foundation. This paper addresses this issue with a set of design guidelines for some crucial parameters in GW SHM systems, backed by the theoretical reasoning for each. First, guidelines pertaining to the excitation signal are outlined for choice of modulation window, number of cycles, frequency, and GW mode. Then, selection of transducer dimensions under practical constraints is covered in detail for isotropic structures. Theoretical models have been developed and validated earlier by the authors that capture the transduction mechanisms of GWs using piezoelectric transducers. This paper exploits those models for their optimal design in GW SHM. The different possible piezoelectric transducer types and configurations are outlined, and the applicability of each to different scenarios is described. Finally, other design issues for GW SHM are briefly discussed.*

Keywords*: structural health monitoring, guided waves, damage prognosis, design guidelines, piezoelectric transducers*

1. INTRODUCTION

The vision of having damage prognosis capabilities in aerospace, civil and mechanical systems has created a lot of interest in structural health monitoring (SHM) over the past decade or so. SHM should enable regular scans of the structure for damage and warnings for the user in near-real time about any incipient damage. It should also be able to tie in with prognostic algorithms to furnish estimates about the remaining service life of the structure, thereby increasing safety. It could enable a transition from schedule-driven inspection to condition-based maintenance. The monetary and labor savings benefits that could be accrued may also be very significant.

1.1. Guided-wave structural health monitoring

Among various alternatives under investigation for SHM, there are guided-wave (GW)-based approaches. GWs can be defined as stress waves forced to follow a path defined by the material boundaries of the structure. For example, when a beam is excited at high frequency, stress waves travel in the beam along its axis away from the excitation source, i.e., the beam "guides" the waves along its axis. Similarly, in plates, the GW paths are forced to be within the plane of the plate. These approaches essentially involve exciting the structure with a high frequency burst signal, which sends out a GW pulse in it. By processing the difference in structural response with respect to a baseline signal for the pristine condition, damage can be detected (typically based on some signal energy measure relative to a threshold). If damage is determined to be present, some pattern recognition algorithm trained by empirical/theoretical data can be used to characterize it in terms of type and severity. Some of the approaches can be used to locate the damage as well. While several transducers have been tested, piezoelectric wafer transducers (hereafter referred to as "piezos") seem to be the most commonly used option. This is largely because of the low mass and space penalty associated with incorporating them (crucial in aerospace structures) and their superior energy density for high frequency applications. A detailed survey of GW SHM, including fundamentals and early history, is presented in a review paper by the authors (Raghavan and Cesnik, 2007a).

1.2. Motivation for design guidelines

GW theory is complex due to the dispersive nature of these waves and the fact that at least two modes can propagate at any frequency. In composite materials, this is further complicated by the directional dependence of wavespeeds and excitability. Therefore, a good understanding of GW theory and a fundamental characterization of the nature of GWs generated and detected by piezos in various structural configurations is very desirable. The theory of free GW propagation in isotropic, anisotropic and layered materials for various geometries as well as excitation using conventional NDE ultrasonic transducers is well-documented (Rose, 1999). The problem of modeling GW excitation by surface-bonded piezos was largely not considered until recently. Consequently, little or no theoretical basis is provided by researchers for their choice of the various testing parameters involved such as transducer geometry, dimensions, location and materials, excitation frequency, bandwidth among others. Three-dimensional (3-D) elasticity models were developed by the authors (Raghavan and Cesnik, 2005; 2007c) to capture the GW field excited by surface-bonded piezos in isotropic plate structures. These were supported by finite element method (FEM) simulations and

experimental tests to verify them. More recently, an extension of this theoretical model for multi-layered, fiber-reinforced composite plates was also proposed by the authors (Raghavan and Cesnik, 2007b). The present work seeks to exploit these models along with other concepts to furnish a set of design guidelines for GW SHM systems, specifically for the excitation signal and the transducers in isotropic structures. Figure 1 shows a tree-diagram which lists the various parameters that need to be chosen for the excitation signal and transducers in GW SHM systems. The next two sections prescribe the specific guidelines for excitation signal and transducer design. Each sub-section in these begins with the guideline in italics, followed by the reasoning behind it.

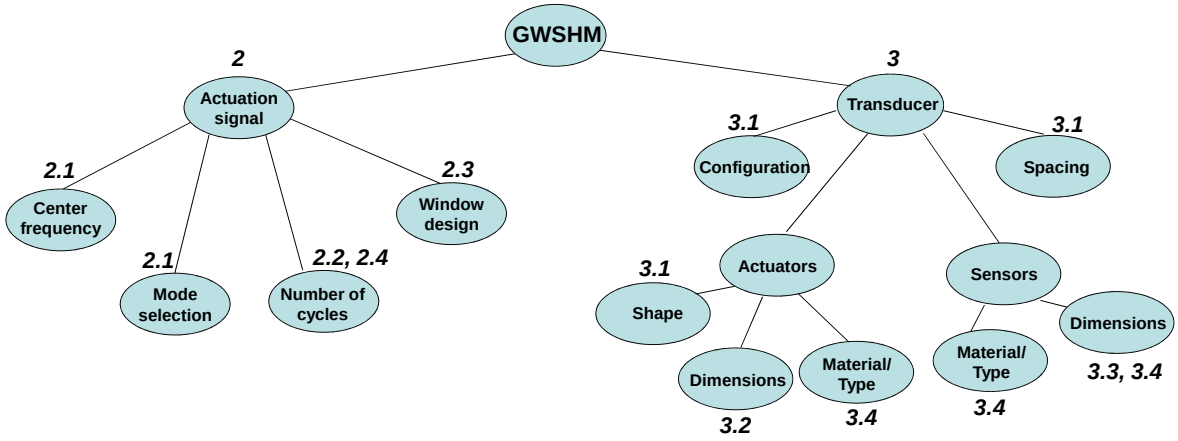

Figure 1: Tree diagram of parameters in GW SHM (number in italics correspond to section numbers)

2. EXCITATION SIGNAL

As mentioned in the introductory section, the excitation signal is typically a high-frequency pulse signal. This feature distinguishes this approach from other vibration-based SHM schemes. If the excitation signal is too long in the time-domain, the response of the structure might be masked by multiple boundary reflections. Most commonly, a modulated sinusoidal toneburst signal spanning a few cycles is used. The following guidelines should aid in choosing the specifics of this signal.

2.1. Center frequency/GW mode

The center frequency and GW mode should be decided based on the defect types(s) of interest, using relevant information of GW sensitivity studies for each defect type.

The center frequency of the excitation signal is a crucial parameter. Depending on the mode, the GW wavelength depends on it, which in turns defines the minimum size of the least sensitive of the different defect types which are hoped to be detected using the GW SHM system. The wavelengths of the GWs are found from the dispersion curves. The dispersion curves for an isotropic plate of thickness $2b$ with Lamé's moduli λ and μ and density ρ, are generated from the solutions of the following transcendental equation:

$$\frac{\tan \beta b}{\tan \alpha b} = \frac{-4\alpha\beta\xi^2}{(\xi^2 - \beta^2)^2} \tag{1}$$

where

$$\alpha^2 \equiv \frac{\omega^2}{c_1^2} - \xi^2 \;\; ; \;\; \beta^2 \equiv \frac{\omega^2}{c_2^2} - \xi^2$$
$$c_1 = \sqrt{\frac{\lambda + 2\mu}{\rho}} \;\; ; \;\; c_2 = \sqrt{\frac{\mu}{\rho}} \tag{2}$$

and $\xi = 2\pi/\lambda$, λ being the wavelength of the GW and ω being the angular frequency of excitation. A typical dispersion curve (phase velocity versus frequency-thickness product) is shown in Figure 2. In composites, a more intricate matrix

equation needs to be solved to obtain the dispersion curves, which also depend on angle of propagation (Raghavan and Cesnik 2007b). Mode sensitivity to a defect can be found using FEM-based defect sensitivity studies or from theoretical models that describe the GW-scattered field from the defect (e.g., Alleyne and Cawley 1992, Chang and Mal 1999, Grahn 2003, Guo and Cawley 1993, Fromme et al. 2004). For example, by exciting a mode with a through-thickness stress profile such that the maximum power is transmitted close to a particular interface through the plate thickness, the plate can be scanned for defects along that interface. Rose et al. (1993) predicted through analysis of displacement and power profiles across the structural thickness that in metallic plates the S_0 mode would be more sensitive to detect large cracks or cracks localized in the middle of the plate. On the other hand, the S_1 mode would be better suited for finding smaller cracks or cracks closer to the surface. Alleyne and Cawley (1992) found from FEM-based sensitivity studies that notches of depth of the order of 1/40 times the wavelength could be detected by Lamb waves in a plate. They also found that the sensitivity was independent of the size of the notch in the plane of the plate, as long as the defect was small compared to the wavelength. Furthermore, it might be useful to test at more than one frequency, since defects of some particular dimensions can be insensitive to a given wavelength (see, e.g., Fromme et al. 2004).

The following types of structural damage/defects have been detected using GWs in the literature: delaminations in composites (Guo and Cawley 1993), notches (Alleyne and Cawley 1992), impact damage (usually in the form of an indentation or hole – e.g., Fromme et al. 2004, Raghavan and Cesnik 2007d), structural cracks (which could be fatigue-induced, e.g., Chang and Mal 1999), loss of material due to corrosion (e.g., Thomas et al. 2004), cracks in welds (e.g., Jones et al. 2004), bolt torsion in clamps/fasteners supporting structures (e.g., Derriso et al. 2004), disbonds between skin and the honeycomb core in sandwich structures (e.g., Blaise and Chang 2004), and disbonds at adhesive joints (e.g., Matt et al. 2005).

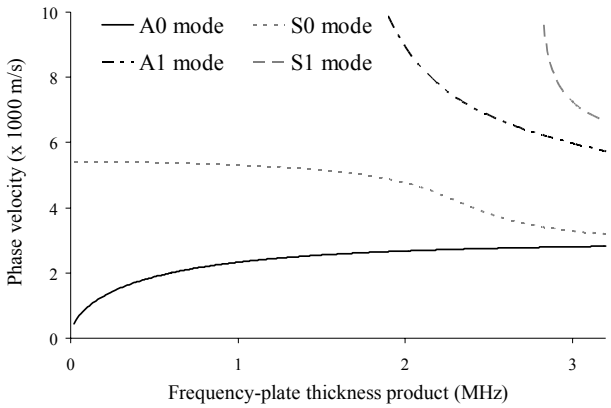

Figure 2: Phase velocity dispersion curve for aluminum alloy plates (E = 70 GPa, υ = 0.3, ρ = 2700 kg/m^3)

2.2. Number of cycles

Decide on the number of cycles in the toneburst based on a tradeoff study between blind-zone area and dispersiveness.

There is always a small blind-zone area surrounding the transducers used in GW SHM, where damage cannot be detected. The blind-zone area results because small amplitude scattered GWs from defects going to the sensor cannot be easily separated from the large amplitude first transmitted GW pulse from the actuator (or the excitation signal if the actuator itself is being used as sensor) or from the GW reflections from the boundary (which are also usually significantly larger compared to reflections from defects). Therefore, from this standpoint, a smaller number of cycles will decrease the blind zone area. On the other hand, a larger number of cycles will reduce the frequency bandwidth, and thereby, decreases "dispersion." Dispersion is a phenomenon wherein the original signal is distorted as it travels in a medium due to the different wavespeeds of its component frequencies. Therefore, the number of sinusoidal cycles in the excitation signal has to compromise between these two factors. The former is proportional to the square of the number of cycles for a given excitation frequency while the latter reduces with increasing number of cycles due to the reduction of the main lobe width in the frequency spectrum. Thus, if one is operating in a relatively non-dispersive region of the dispersion curve, one could afford to use a fewer number of cycles.

2.3. Modulation window

Choose a Kaiser window for modulating the excitation signal.

To minimize the problem of dispersion created by using a finite time-duration signal, it should be modulated by a window which minimizes the spread of the signal in the frequency domain. The effect of truncating a harmonic signal is to smear its signal energy in the frequency domain in a main lobe centered about the original frequency, along with

weaker side lobes. Modulation typically widens the main lobe and makes the side lobes smaller. The *Kaiser window* approximates the prolate spheroidal window, for which the ratio of the main-lobe energy to the side-lobe energy is maximized in the frequency domain (Papoulis 1984). It is given by the expression:

$$k(t) = \frac{I_0\left(\beta\sqrt{1-\frac{4t^2}{\tau^2}}\right)}{I_0(\beta)} \tag{3}$$

where $I_0(\ )$ is the modified Bessel function of the first kind of order 0, τ is the duration of the window (fixed by the number of cycles) and β is a parameter that controls the main lobe width in the frequency domain. Let Δ_{ml} be the chosen main lobe width defined by the distance between the central zero-crossings in the plot of the magnitude of the Fourier transform (see Figure 3). Then the amplitude attenuation factor in dB of the main lobe to the largest side lobe is:

$$A_{sl} = \frac{155\Delta_{ml}\tau - 1}{24\pi} - 12 \tag{4}$$

The window parameter β is chosen to be:

$$\beta = \begin{cases} 0 & A_{sl} \le 13.26 \\ 0.76609(A_{sl} - 13.26)^{0.4} + 0.09834(A_{sl} - 13.26) & 13.26 < A_{sl} < 60 \\ 0.12438(A_{sl} + 6.3) & 60 \le A_{sl} < 120 \end{cases} \tag{5}$$

That is, for $A_{sl} \le 13.26$, the Kaiser window reduces to the rectangular window.

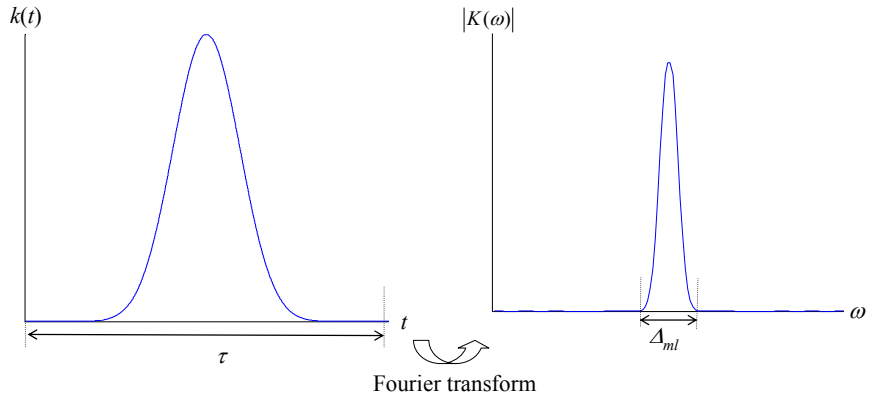

Figure 3: The Kaiser window and its Fourier transform

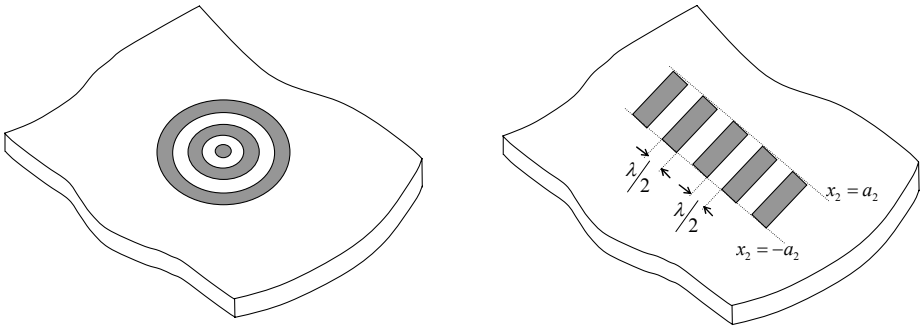

Figure 4: Illustration of comb configurations – a) using ring elements (left) and b) using rectangular elements (right)

2.4. Excitation signal for comb array configurations

When using a comb transducer, ensure that the main lobe in the frequency spectrum is narrow enough so that higher harmonics of the primary wavenumber of interest are not excited.

A comb configuration (Figure 4) is an array of transducers that is equally tuned to a particular wavelength of interest and its integer multiples (illustrated in Figure 5). Therefore, when using such a configuration, ensure that the excitation signal is such that its frequency bandwidth does not include any higher harmonics of the wavelength of interest. A more detailed description of comb transducers can be found in Section 3.

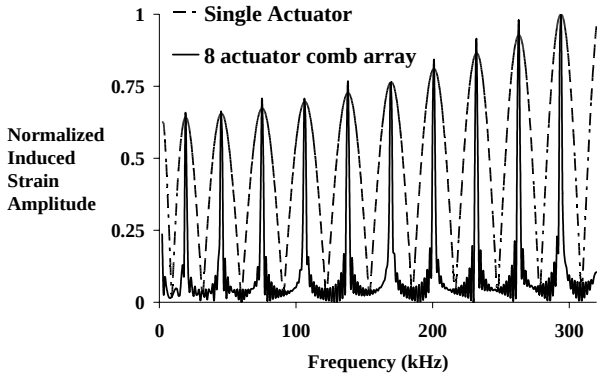

Figure 5: Comparison of harmonic induced strain in A_0 mode between an 8-array piezo comb transducer and that of a single piezo-actuator (power is kept constant).

3. TRANSDUCER DESIGN

3.1. Configuration/shape selection

Choose the configuration of the transducer(s) and the individual transducer shape(s)/type(s) to suit the application:

- *For large area scanning from a central point on the structure, use multi-element arrays*
- *For small area scanning, use a few elements in pulse-echo or pitch-catch mode*
- *For uniform radiation in all directions, use circular actuators*
- *For focused radiation, use an appropriately designed rectangular piezo actuator*
- *For unidirectional sensing, use a Macro Fiber Composite (MFC) transducer*
- *For modal selectivity, use comb configurations*

The configuration and shape are highly dependent on the application area. For example, if large area scanning from a central point of a structure without structural obstacles (such as a reinforcement or joint) is desired, a linear phased or circular array may be preferable. Phased arrays operate by scanning individual sector angles by applying appropriate delays and scaling factors to the excitation signals to the individual array transducer elements (see e.g., Purekar et al. 2004). If however, a smaller area is to be monitored, a simpler solution is to use a few transducers operating in the pulse-echo configuration. A minimum of three transducers are needed for triangulation in a plate or shell-like structure (see e.g., Raghavan and Cesnik 2007d). The pitch-catch configuration requires a denser network of transducers in order to allow for triangulation. For beam-like structures, two transducers in the pulse-echo configuration suffice to locate the damage. Note that the notion of "small" and "large" areas depends on the material damping characteristics as well as the power available per actuator. The relative spacing between sets of transducers on the structure should be based on a calibration experiment to get an estimate of the range capability of the chosen actuator/sensor configuration for the structure of interest and actuation voltage levels.

The radiation patterns of a particular actuator depend on its shape. To ensure uniform radiation in all directions in the plane of the plate, use circular actuators. This is crucial in linear phased arrays, for example. If it is desired to monitor one or more particular area(s) of the structure selectively, focused actuator shapes such as rectangular ones are preferable. An anisotropic piezocomposite actuator, such as MFC actuator (see Figure 6), may also be useful in this regard due to its preferential direction of radiation along its fibers (though care should be taken in their design since these also excite horizontally polarized shear (SH-) modes along with Lamb modes, see Raghavan and Cesnik 2007c). They are also advantageous to use in certain applications due to their unidirectional sensing capability along the fiber direction. To achieve modal selectivity and thereby easier signal interpretation, a comb configuration would be much preferable. See Figure 7 for illustrative harmonic out-of-plane displacement GW fields by a MFC actuator.

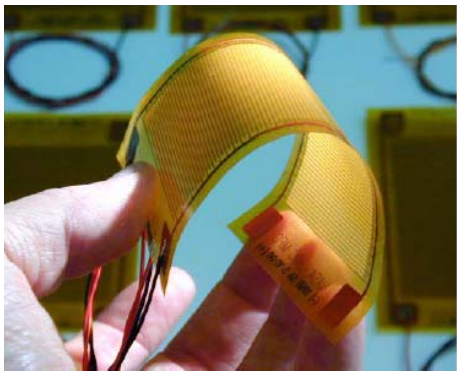

Figure 6: The packaged MFC (Wilbur and Wilkie 2004).

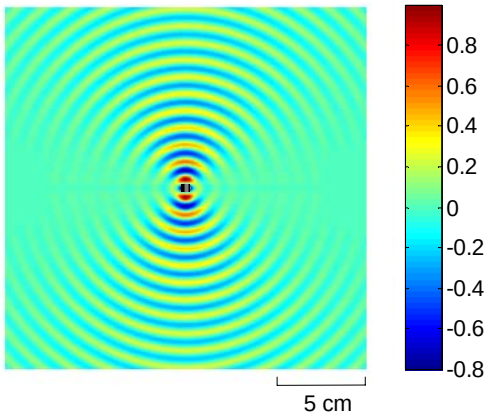

Figure 7: Harmonic radiation field (out-of-plane displacement) due to a MFC actuator 100 kHz , A_0 mode in a 1-mm thick aluminum plate (the actuators are at the center, on either free surface, of size 0.5 cm × 0.5 cm with the fibers along the vertical direction)

3.2. Actuator size

Determine the optimal size of the actuator based on the theoretical model corresponding to the particular chosen shape.

The formulas in this section are based on theoretical models developed by the authors (Raghavan and Cesnik, 2005; 2007c) and assume the circulation power formula for harmonic excitation with capacitive loads (in this case, the piezo-actuators), i.e., $P = 2\pi fCV^2$. In practice, for modulated sinusoidal tonebursts, the peak power drawn is close to this value. For more accuracy, a correction factor can be used depending on the modulation window. It should be noted that, since capacitive loads are reactive, this power is used in the positive half-cycle for charging the capacitance and is gained back in the negative half-cycle when the capacitance is discharged. The power dissipated in exciting the GW field in the structure is neglected, since that is several orders of magnitude smaller than the reactive power. In addition, the nonlinear dependence of the capacitance of piezoelectric elements on driving voltage and frequency is neglected (see e.g., Jordan et al. 2000). This should be accounted for at high driving voltages (> 30 V). Sizing guidelines for circular, rectangular and ring-shaped comb actuators are covered in this paper. However, the reasoning can be extended to design MFCs and comb configurations using rectangular piezos. The objective of the design process here is to maximize the GW field strength while remaining within the power, voltage and maximum actuator size constraints of the system. The different parameters needed in the formulas below are:

System constraints:
V_{max} = Maximum actuation voltage that can be applied by the power source
P = Maximum power that can be supplied by the power source
a_{max} = Maximum allowable actuator dimension
Actuator properties:
k = Dielectric ratio of the actuator material
h_a = Thickness of actuator along the direction of polarization
Structural (substrate) properties:
E = Young's modulus of the isotropic plate structure
υ = Poisson's ratio of the isotropic plate structure
ρ = Material density of the isotropic plate structure
$2b$ = Thickness of the plate structure
Other constants/parameters:
ε_0 = Permittivity of free space
f = Center frequency of excitation
ξ = Wavenumber of the chosen guided wave mode for the center frequency used, found using Eq. (1)

A. Circular actuator uniformly poled through thickness:

Let a be the variable corresponding to the radius of the circular actuator. Also, consider the parameter a_0 such that

$$a_0 = \frac{1}{\pi V_{\max}} \sqrt{\frac{Ph_a}{2k\varepsilon_0 f}} \tag{6}$$

Figure 8 illustrates the design space and the geometric locations of a_0 and other parameters that will be discussed for the circular actuator. Thus. a_0 is the value of a at the intersection of the power constraint curve and the line $V = V_{\max}$. If $a_0 < a_{\max}$, which is the maximum radius of an actuator permissible by the designer, then:

1. If $a = a_0$ corresponds to an extremum of $|J_1(\xi a)|$, then choose this value as actuator radius.
2. If $a = a_0$ does not correspond to an extremum of $|J_1(\xi a)|$, let a_2 correspond to the first extremum of $|J_1(\xi a)|$, such that $a_0 < a_2 \le a_{\max}$, if it exists (else choose $a_2 = a_{\max}$) and let a_1 correspond to the maximum value of $|a.J_1(\xi a)|$ for $0 < a \le a_0$. This is because, as shown in our earlier work (Raghavan and Cesnik 2005), the GW strain field strength is linearly proportional to $a.J_1(\xi a)$.

If

$$a_1.J_1(\xi a_1)V_{\max} > J_1(\xi a_2).\sqrt{\frac{Ph_a}{2\pi^2 k\varepsilon_0 f}} \tag{7}$$

then choose $a = a_1$. Otherwise, choose $a = a_2$. If $a_0 > a_{\max}$, then choose the largest maxima of $|a.J_1(\xi a)|$ with $0 < a \le a_{\max}$, if such a maximum exists, else choose a to be $a_{\max}$.

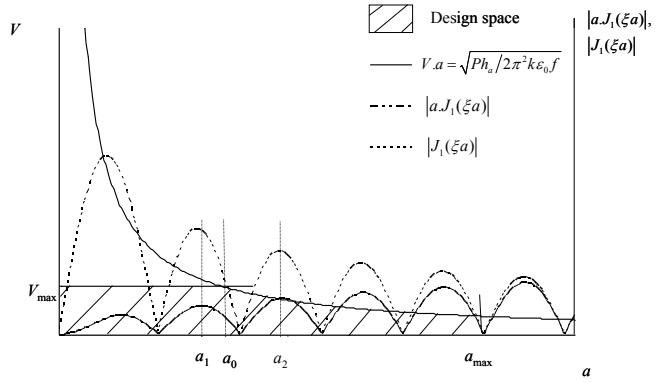

Figure 8: Parameters and design space for circular actuator dimension optimization

B. Rectangular actuator uniformly poled through thickness:

In this case, the dimensions depend on the direction(s) in the plane of the structure where radiation is to be maximized. If, for example, it is desired to maximize radiation along a particular direction while minimizing radiation perpendicular to it, then the rectangular actuator should be oriented such that one of its two axes of symmetry is along the direction of interest, say x_1. Let the dimensions of the actuator be $2a_1$ along x_1 and $2a_2$ perpendicular to it, with $a_1 < a_2$ (see Figure 9).

Consider $2a_{\max}$ to be the maximum allowable actuator dimension. As shown in Figure 10, choose a_{2o} (the optimal value for a_2) to be the largest zero of $\sin \xi a_2$ such that $0 < a_2 \le a_{\max}$, if it exists. If no such zero exists then choose $a_2 = a_{\max}$.

Let

$$a_0 \equiv \frac{Ph_a}{8\pi a_2 k\varepsilon_0 f V_{\max}^2} \tag{8}$$

If this value of a_0 is larger than or equal to $a_{\max}$, reset a_0 to be $a_{\max}$. If there exists $\tilde{a}$ corresponding to an extremum of $|\sin \xi a_1|$ such that $0 < \tilde{a} \le a_0$, then choose the smallest value of $\tilde{a}$ for a_1. If such an extremum does not exist, and a_0 was reset to $a_{\max}$, then choose $a_1 = a_{\max}$.

If such an extremum does not exist, and $a_0 < a_{\max}$, then let a_t be the first extremum of $\left|\sin \xi a_1 / \sqrt{a_1}\right|$ such that $a_0 < a_t \le a_{\max}$. If such a_t does not exist, choose $a_t = a_{\max}$. If

$$\sin(\xi a_0) V_{\max} > \sin(\xi a_t) . \sqrt{\frac{P h_a}{8\pi a_t a_2 k \varepsilon_0 f}} \tag{9}$$

then the optimal value of a_1 is $a_{1o} = a_0$, else choose $a_{1o} = a_t$. The locations of these parameters in the design space are shown in Figure 11.

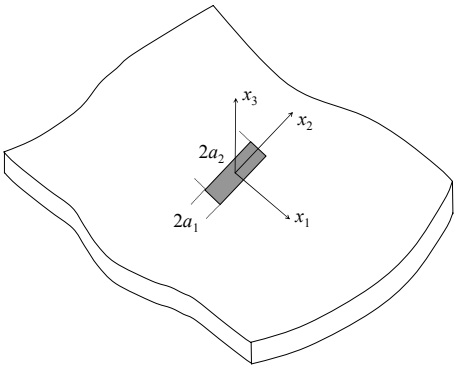

Figure 9: Parameters and coordinate axes for rectangular actuator

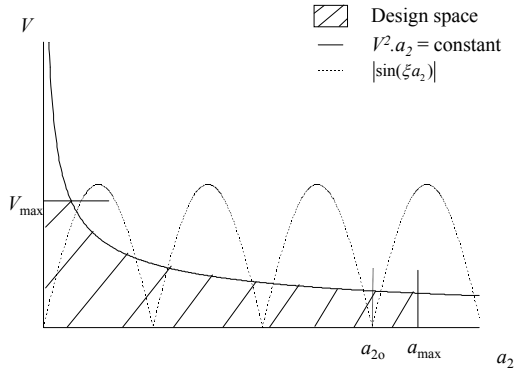

Figure 10: Choice of a_2 for rectangular actuator

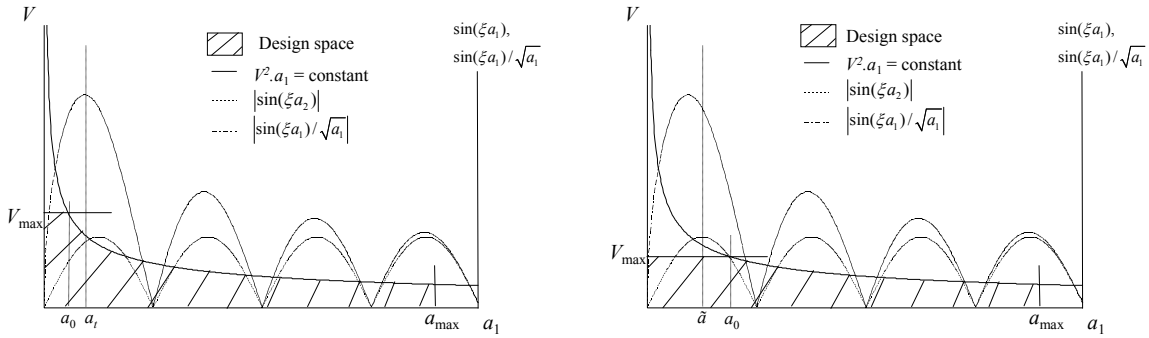

Figure 11: Possible optimal choices of a_1 for rectangular actuator in two possible cases

C. *Ring-shaped comb actuator uniformly poled through thickness:*

The possibility of using this configuration arises only if $a_{\max}$, which is the maximum allowable actuator radius, is larger than the value of a corresponding to the second extremum of $\left|a.J_1(\xi a)\right|$. A comb configuration can be achieved by using individual ring-shaped actuators or by using a large circular actuator with the necessary electrode pattern etched on it. A comb configuration is much more preferable compared to a circular actuator for axisymmetric GW excitation due to its modal selectivity. In designing this, the maximum number of ring shaped actuators that can be used is n–1 where n is the number of extrema of $\left|a.J_1(\xi a)\right|$ for $a \le a_{\max}$. If n is odd and greater than 1, there can be one circular actuator and n–2 ring-shaped actuators. If n = 1, only one circular actuator can be used. The internal and external radii of the rings are the values of a corresponding to the extrema of $\left|a.J_1(\xi a)\right|$. In choosing the number of ring actuators n, the only issue preventing one from using the maximum possible number of elements within the allowable actuator size is the drop in amplitude due to increase in capacitance as more rings are used (which may cause reduced actuation voltage due to the finite power supply of the system). Hence, the choice of n should be made after a careful tradeoff study between tolerable dispersiveness and signal amplitude for each possible n.

3.3. Sensor size

Choose the sensor dimensions in the plane of the plate to be minimal, preferably much smaller than the half-wavelength of the GW.

Theoretically, it can be proven that the sensor response keeps increasing as the sensor dimensions in the plane of the plate are reduced, assuming the sensor is in the far-field relative to the source (a distance greater than ten wavelengths or so, see Raghavan and Cesnik 2005). The only constraint on decreasing sensor size is the phenomenon of shear lag wherein all the strain is taken by the bond layer and nothing is transmitted to the sensor. However, with a reliable bond layer, this limit can be stretched to a considerable extent. The exact smallest value beyond which shear lag dominates may have to be determined experimentally for a particular bonding mechanism[1].

Thus, it is evident that the optimal dimensions for sensors and actuators are quite different. This ideally leads to separate actuators and sensors should be used for improved signal performance. However, the final decision should be made in view of the system architecture under consideration.

3.4. Transducer material

Choose the actuator material with the highest value for the product of in-plane Young's modulus and piezoelectric constant (the relevant d-constant) divided by the dielectric constant. Use a sensor material with the highest value for the piezoelectric constant (the relevant g-constant) and minimum material density.

The actuation authority of the piezo increases linearly with increasing values of piezoelectric constant (d_{31} or d_{33} depending on whether a piezo with isotropic poling or an anisotropic piezocomposite, such as MFC actuator, is used) and in-plane Young's modulus (Y_a^{11} or Y_a^{33}). The reactive circulation power increases linearly with increasing dielectric constant *k.* Thus to maximize the actuation capability per unit power drawn, the material with maximum value for the ratio $Y_a^{11} d_{31} / k$ (or $Y_a^{33} d_{33} / k$, as appropriate) should be chosen.

The sensor response strength is directly proportional to the product of the in-plane Young's modulus, the piezoelectric constant and sensor thickness (Raghavan and Cesnik 2005). However, it is not advisable to increase sensor thickness or Young's modulus beyond a point. This may cause the sensor to significantly disturb the guided wave field being sensed, and the measured output will not be representative of the incident GW field. This is directly related to the relative thickness and relative Young's modulus of the sensor to the substrate. Thus, for minimum interference with the GW field, PVDF sensor elements would be more suitable due to their finer thickness and low in-plane Young's modulus, however their response strength is usually weak and often piezoceramics are preferred. This relates to the classical problem of the science of measurements, wherein one has to compromise between sensor readability and fidelity. However, an increase in the *g*-constant does not perturb the field and at the same time increases sensor response. The higher the material density, the greater the mass of the sensor, thereby perturbing the guided wave field without any increase in the sensor response. Hence, the sensor material with minimum material density is preferable.

4. CONCLUDING REMARKS

The actuation signal and transducers, for which detailed recommendations were provided in this paper, are just two of the many pieces in GW SHM systems. There are several other critical design issues involved in a successful GW SHM system. For example, the bond layer should be thin, stiff (at frequency of interest), uniform, and robust to environmental conditions to ensure good transmission of strain between the transducer and substrate. There are decisions concerning the electrical architecture, such as whether wireless connections are needed. If wires are used, the connections should be able to withstand electromagnetic interference and electrical noise (e.g., by using co-axial cables). Several other such issues exist in other areas of GW SHM such as signal processing, pattern recognition, actuation hardware, system reliability, transducer diagnostics, etc. In many of these, because GW SHM is still evolving, it might not be possible to obtain clear-cut design guidelines at this point. Some insights and recommendations for the signal processing algorithm and elevated temperature effects can be found in other work by the authors (Raghavan and Cesnik 2007d, 2007e). Efforts by various researchers in other areas of the problem have been covered in a review paper by the authors (Raghavan and Cesnik, 2007a). It is hoped that this set of design guidelines will inspire similar efforts for other areas of GW SHM.

5. ACKNOWLEDGEMENTS

The authors are grateful to William Prosser (NASA Langley), Lance Richards and Larry Hudson (NASA Dryden), and John Lassiter (NASA Marshall) for their comments. This work is supported by the Space Vehicle Technology

[1] In the authors' experience, using a two-part overnight setting epoxy (Epotek-301 from Epoxy Technology) with piezos of thickness 0.3 mm on a 3.2-mm aluminum plate, beyond an in-plane size of 0.5 cm, sensor size reduction does not yield any advantage.

Institute under grant NCC3-989 jointly funded by NASA and DoD within the NASA Constellation University Institutes Project, with Ms. Claudia Meyer as the project manager.

6. REFERENCES

Alleyne, D.N. and Cawley, P., 1992, "The Interaction of Lamb Waves with Defects", IEEE Transactions on Ultrasonics, Ferroelectrics and Frequency Control, Vol. 39, No. 3, pp. 381-396.

Blaise, E. and Chang, F.-K., 2002, "Built-in Damage Detection System for Sandwich Structures under Cryogenic Temperatures", Proc. SPIE Symposium on Smart Structures/NDE, Vol.. 4701, pp. 97-107, San Diego, U.S.A.

Chang, Z. and Mal, A.K., 1999, "Scattering of Lamb Waves from a Rivet Hole with Edge Cracks," Mechanics of Materials, Vol. 31, No. 3, pp. 197-204.

Derriso, M.M., Olson, S., Braisted, W., DeSimio, M., Rosenstengel, J., and Brown, K., 2004, "Detection of Fastener Failure in a Thermal Protection System," Proc. SPIE Symposium on Smart Structures/NDE, Vol. 5390, pp. 585-596, San Diego, U.S.A.

Grahn, T., 2003, "Lamb Wave Scattering from a Circular Partly Through-thickness Hole in a Plate", Wave Motion, Vol. 37, pp. 63-80.

Guo, N. and Cawley, P., 1993, "The Interaction of Lamb Waves with Delaminations in Composite Laminates", Journal of the Acoustical Society of America, Vol. 94, pp. 2240-2246.

Fromme, P., Wilcox, P., Lowe, M. and Cawley, P., 2004, "On the Scattering and Mode Conversion of the A_0 Lamb Wave Mode at Circular Defects in Plates", Review of Quantitative Nondestructive Evaluation, Vol. 23, eds. D.O. Thompson and D.E. Chimenti, pp. 142-149.

Jones, R., Wallbrink, C., Tan, M., Reichl, P., and Dayawansa, D., 2004, "Health Monitoring of Draglines Using Ultrasonic Waves," Engineering Failure Analysis, Vol. 11, pp. 257-266.

Jordan, T., Ounaies, Z., Tripp, J., and Tcheng, P., 2000, "Electrical Properties And Power Considerations Of A Piezoelectric Actuator," NASA CR-2000-209861/ICASE Report No. 2000-8.

Matt, H., Marzani, A., Restivo, G., Oliver, J., di Scalea, F.L., Kosmatka, J., Sohn, H., Park, G. and Farrar, C., 2005, "A Guided-Wave System For Monitoring The Wing Skin-To-Spar Bond In Unmanned Aerial Vehicles", Proc. XXIII SEM International Modal Analysis Conference, Paper 105, Orlando, U.S.A.

Papoulis, A., 1984, "Signal Analysis", McGraw-Hill, New York

Purekar, A.S., Pines, D.J., Sundararaman, S., and Adams, D.E., 2004, "Directional Piezoelectric Phased Array Filters For Detecting Damage In Isotropic Plates," Smart Materials and Structures, Vol. 13, pp. 838-850.

Raghavan, A. and Cesnik, C.E.S., 2005, "Finite Dimensional Piezoelectric Transducer Modeling for Guided Wave based Structural Health Monitoring", Smart Materials and Structures, Vol. 14 , pp. 1448-1461.

Raghavan, A. and Cesnik, C.E.S., 2007a, "Review of Guided-wave Structural Health Monitoring", The Shock and Vibration Digest, Vol. 39, pp. 91-114.

Raghavan A. and Cesnik C.E.S., 2007b, "Modeling of Guided-wave Excitation by Finite-dimensional Piezoelectric Transducers in Composite Plates," Proc. 15th AIAA/ASME/AHS Adaptive Structures Conference, Paper # AIAA-2007-1725, Honolulu, Hawaii, U.S.A.

Raghavan, A. and Cesnik, C.E.S., 2007c, "3-D Elasticity-based Modeling Of Anisotropic Piezocomposite Transducers For Guided Wave Structural Health Monitoring", to appear in ASME Journal of Vibration and Acoustics (special issue on damage detection and structural health monitoring).

Raghavan, A. and Cesnik, C.E.S., 2007d, "Guided-wave Signal Processing using Chirplet Matching Pursuits and Mode Correlation for Structural Health Monitoring", Smart Materials and Structures, Vol. 16, pp. 355-366.

Raghavan, A. and Cesnik, C.E.S., 2007e, "Studies on Effects of Elevated Temperature for Guided-wave Structural Health Monitoring", Proc. SPIE Symposium on Smart Structures/NDE, Paper # 6529-9, San Diego, U.S.A.

Rose, J.L., 1999, "Ultrasonic Waves in Solid Media", Cambridge University Press, Cambridge, U.K.

Rose J.L., Pilarski A. and Ditri J.J., 1993, "An Approach to Guided Wave Mode Selection for Inspection of Laminated Plate," Journal of Reinforced Plastics and Composites, Vol. 12, pp. 536-544

Thomas, D.T., Welter, J.T., and Giurgiutiu, V., 2004, "Corrosion Damage Detection with piezoelectric wafer active sensors", Proc. SPIE Symposium on Smart Structures/NDE, Vol. 5394, pp. 11-22, San Diego, U.S.A.

Wilbur, M.L., and Wilkie, W.K., 2004, "Active-twist rotor control applications for UAVs," Proc. 24th Army Science Conference, Paper ADM001736, Orlando, Florida, November 29 – December 2

7. RESPONSIBILITY NOTICE

The authors are the only responsible for the printed material included in this paper.